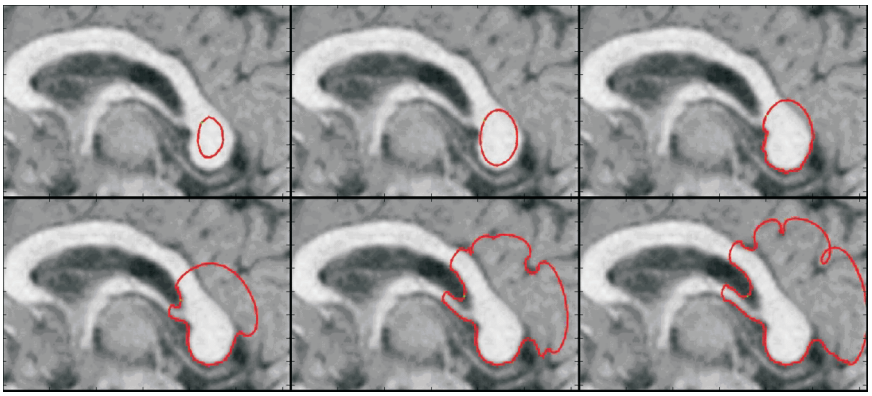

Figure 1. Sample frames (progressing left to right, top to bottom) showing incorrect progress of a deformable model (snake) for segmenting the corpus callosum (CC) in a midsagittal brain magnetic resonance image (MRI), due to the wrong choice of parameters.

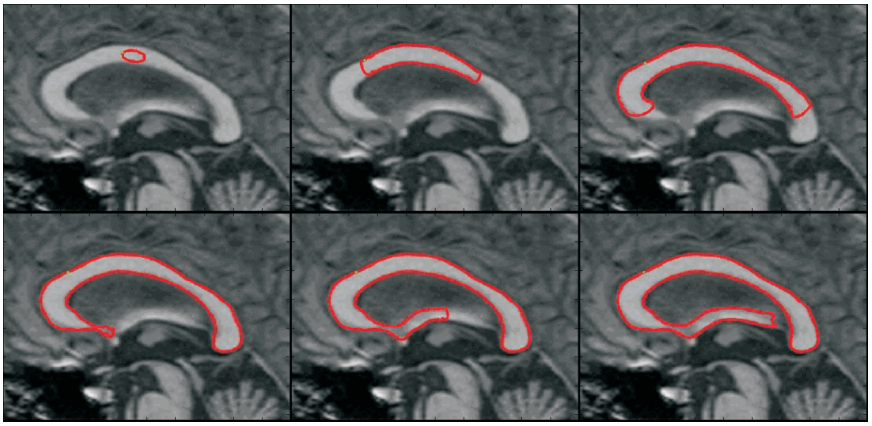

Figure 2. Sample frames (progressing left to right, top to bottom) showing incorrect progress of a snake segmenting the CC in an MRI image. Leaking of the snake occurs because of the weak edge strength (lower left) and incorrect parameter setting.

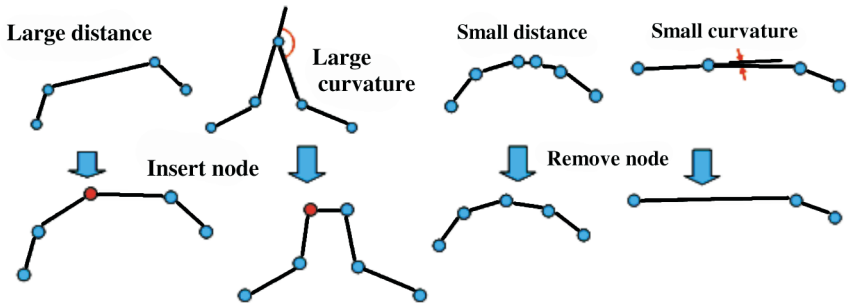

Figure 3. Adaptive resampling of a polygonal snake. (Left) Adding a node if the distance between consecutive nodes is large or curvature is high. (Right) Removing a node if the distance between nodes is small or the curvature is small (appropriate distance and curvature thresholds must be chosen).

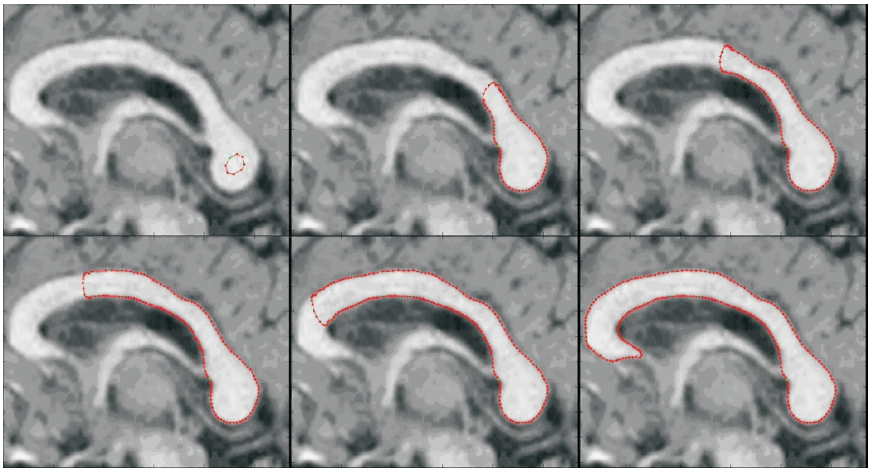

Figure 4. Sample frames (progressing left to right, top to bottom) showing progress of correct snake segmentation of the corpus callosum. The segmentation utilizes adaptive inflation and subdivision and an appropriate choice of weights.

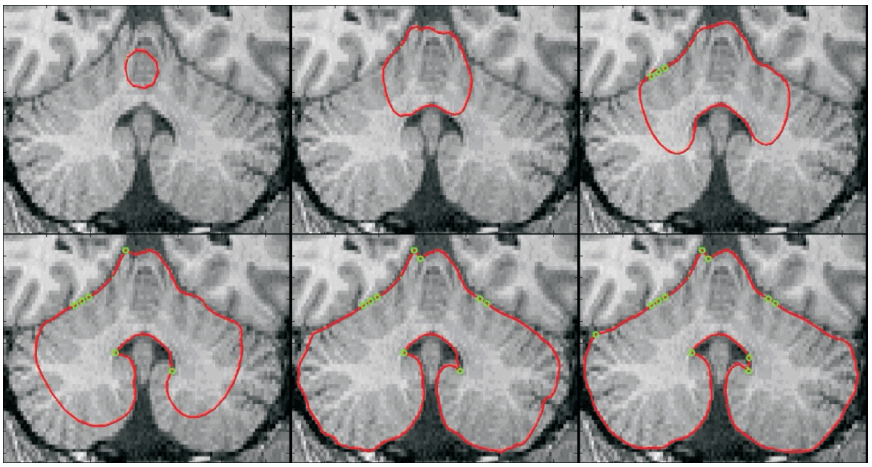

Figure 5. Sample frames showing progress of user-assisted snake segmentation of brain cerebellum. The small green circles are locations of mouse-clicks by the user.

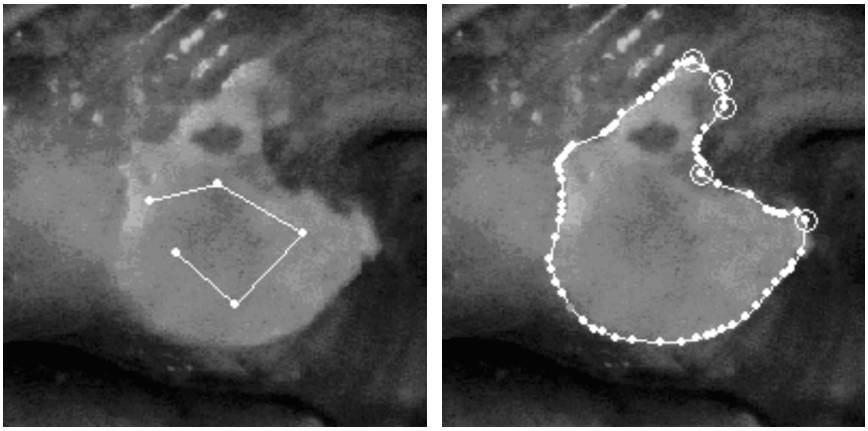

(a) (b)

Figure 6. Segmentation of an oral lesion example using the green band of a digital color image. (a) Initial snake nodes. (b) Final segmentation result (snake nodes shown as white dots and forced points as white circles). Reprinted with permission from [61]. Copyright ©2000, IEEE.

(a) (b) (c)

Figure 7. Gradient Vector Flow Field: (a) original image depicting a corpus callosum in a midsagittal brain MRI, (b) gradient vector field, (c) GVF field. Note how in (c) the field is less sparse than in (b) and smoothly extends outward into homogenous regions.

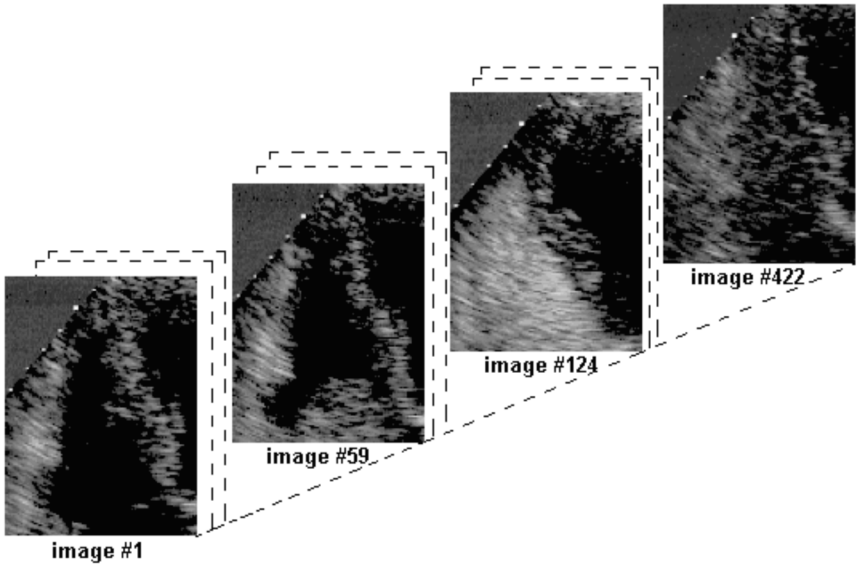

Figure 8. Sample frames from a digitized image sequence. In frame #1, #59, #124, and #422 the contrast agent has not, reached, just reached, totally filled, and washed out from the RV, respectively. Reprinted with permission from [18]. Copyright ©2000, IEEE.

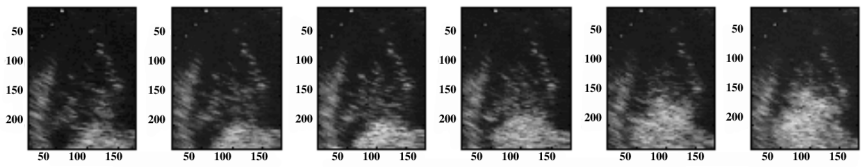

Figure 9. Successive frames of contrast agent entering the right ventricle of the heart. Reprinted with permission from [17]. Copyright ©2000, IEEE.

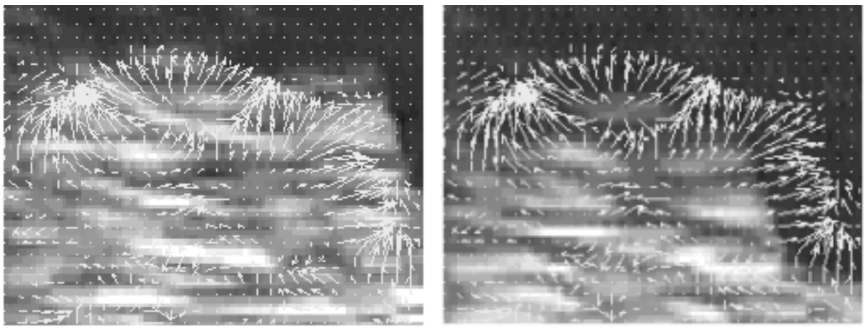

Figure 10. Optical flow (velocity) field shown on two consecutive frames.

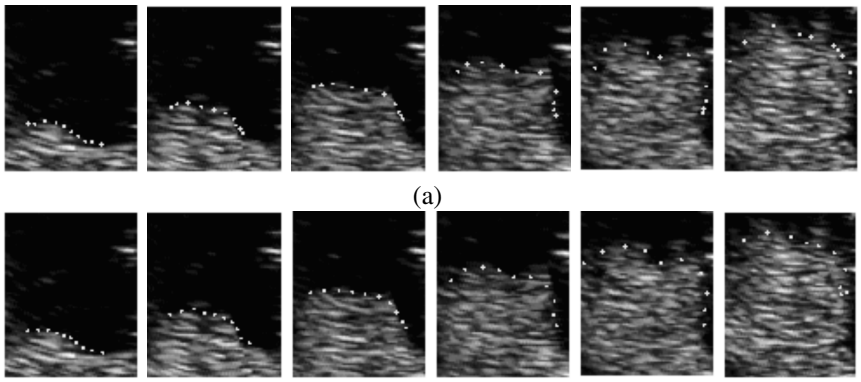

(a)

(b)

Figure 11. Results of tracking a real sequence. Upper frames: without using optical flow forces obtained after 19, 20, 23, 22, 22, and 16 iterations. Lower frames: with optical flow forces obtained after 5, 8, 10, 10, 6, and 10 iterations. Reprinted with permission from [17]. Copyright ©2000, IEEE.

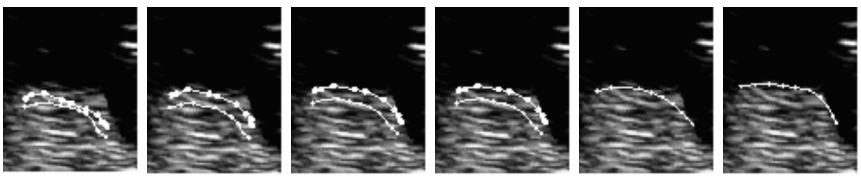

Figure 12. The snake with optical flow forces (large nodes) progresses faster toward the contrast front compared to the snake without optical flow forces. The snake nodes are shown after 1 (left-most), 2, 6, 10, 15, and 23 (right-most) iterations. Reprinted with permission from [17]. Copyright ©2000, IEEE.

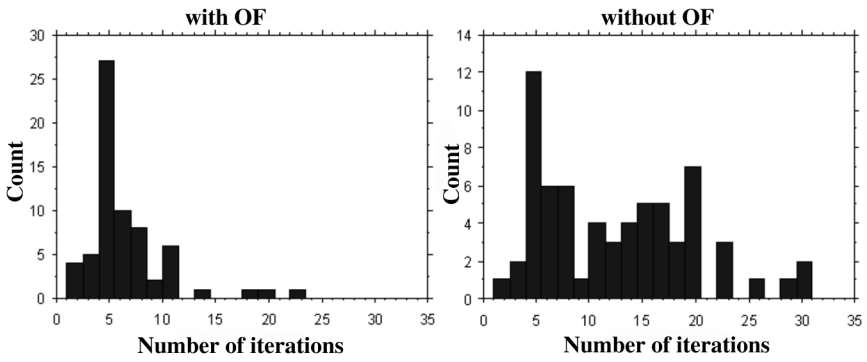

Figure 13. Histogram of the total number of iterations needed for the contour to latch onto the contrast front (a) with optical flow forces and (b) without optical flow forces. Reprinted with permission from [18]. Copyright ©2000, IEEE.

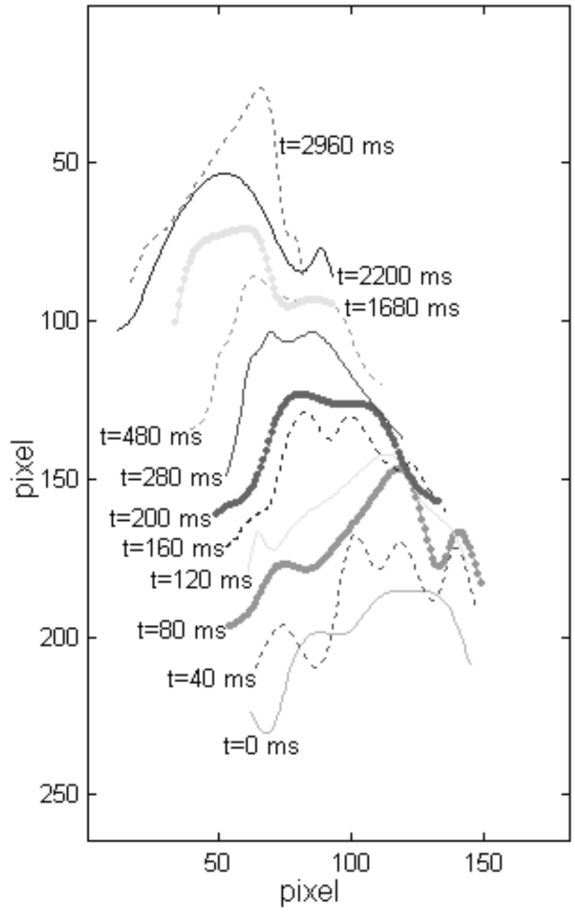

Figure 14. The result of tracking the leading edge in one of the sequences from the ARVD group. Each contour represents the contrast agent front at different times, indicated beside each contour. The contrast front enters the RV ($t = 0$) until the RV is totally filled ($t = 2960$ ms). Note how the contrast front in the initial phase of filling (t = 0 to 480 ms) moves faster than the final phase (t =480 to 2960 ms). This is indicative of the inhomogeneous operation of the RV, identified via contrast front tracking. Reprinted with permission from [18].

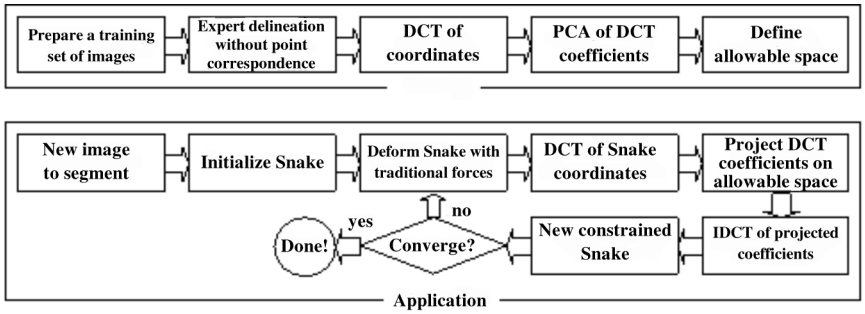

Figure 15. Flowchart depicting the main steps involved in the use of a statistically constrained snake for image segmentation. Reprinted with permission from [62]. Copyright ©2000, IEEE.

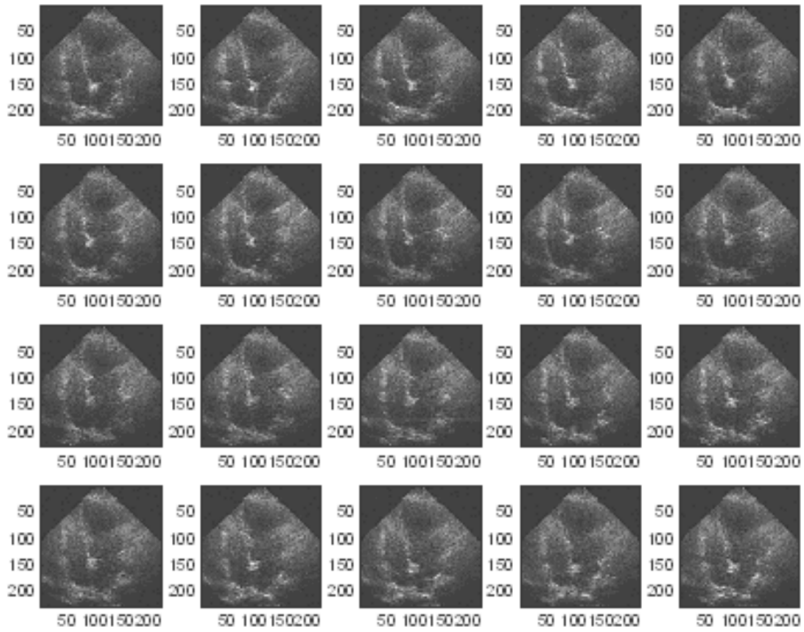

Figure 16. Sample of the echocardiographic training image set.

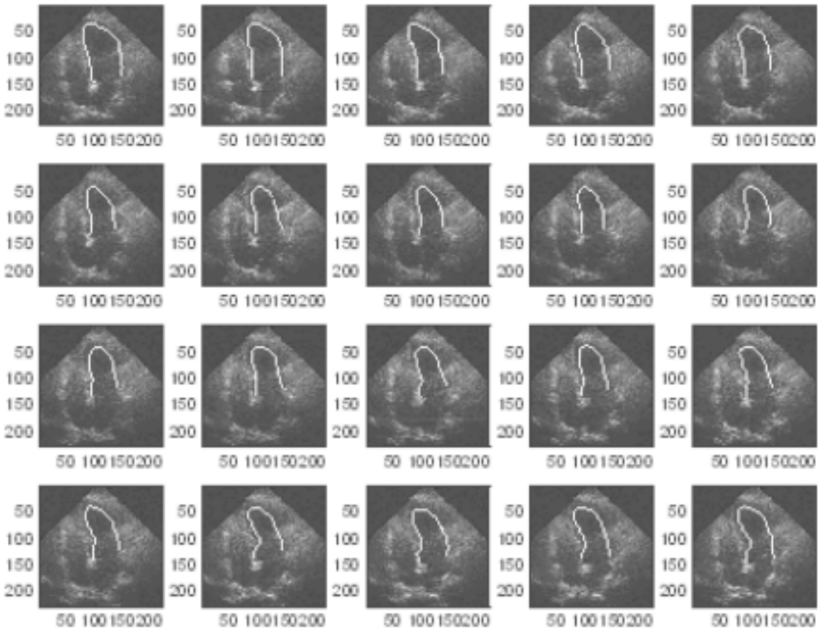

Figure 17. Manual tracings of the LV boundary in the training images.

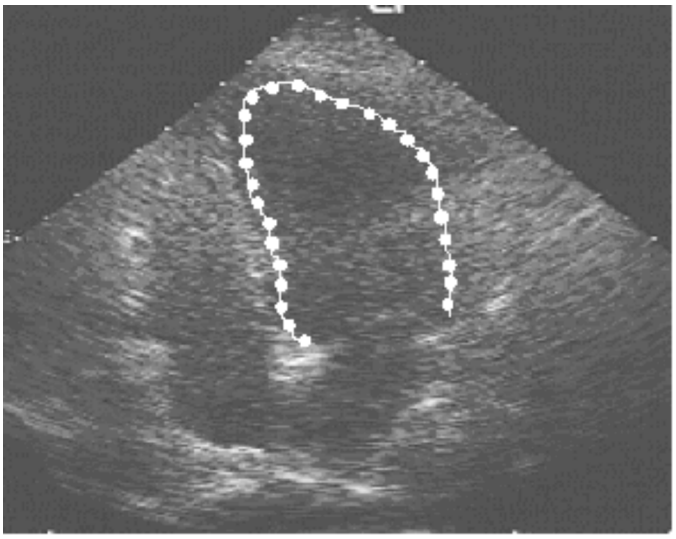

Figure 18. Ultrasound image with manual tracing (continuous) and the contour after IDCT of truncated DCT coefficients (dots). Reprinted with permission from [62]. Copyright ©2000, IEEE.

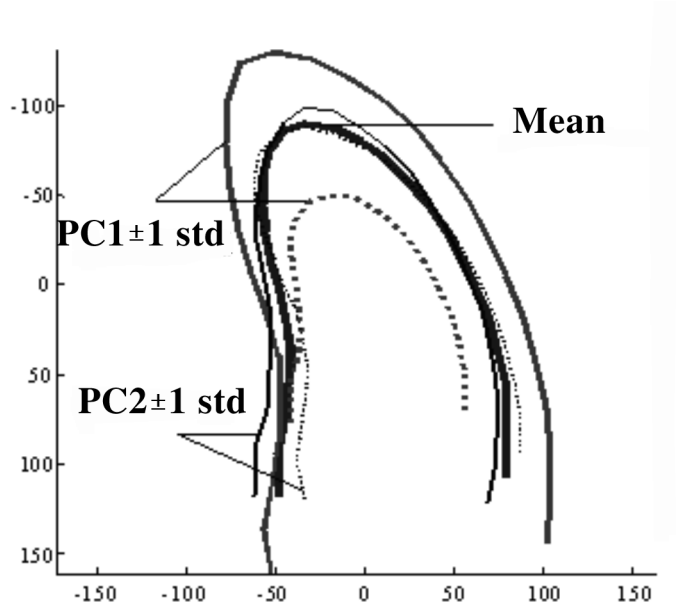

Figure 19. Mean contour and the first and second variation modes (weighted by ± 1 std). Reprinted with permission from [62]. Copyright ©2000, IEEE.

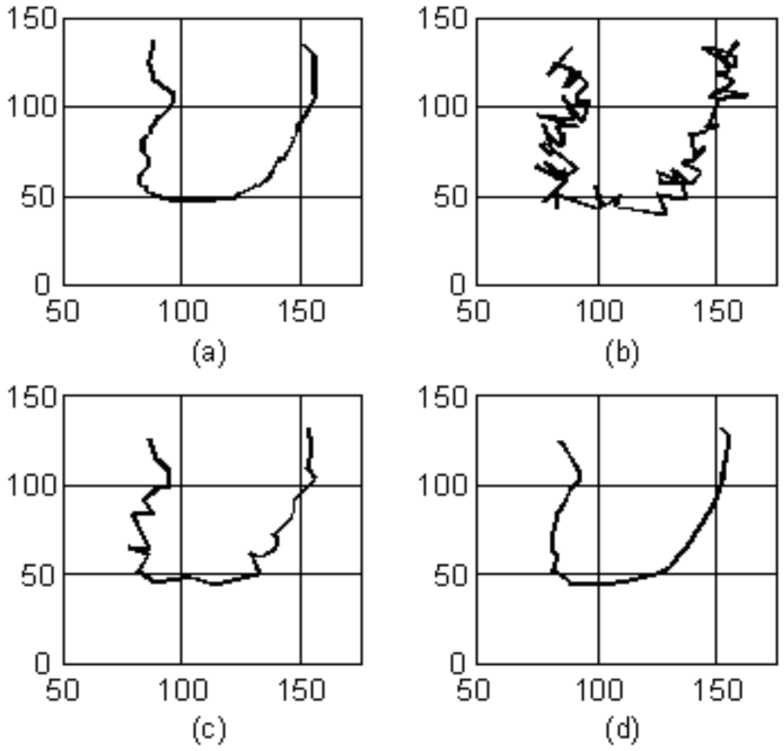

Figure 20. (a) Manual tracing. (b) Noisy version of (a). (c) IDCT of truncated DCT coefficients of (b). (d) Projection of (c) on the allowable shape space (note the similarity to (a)). Reprinted with permission from [62]. Copyright ©2000, IEEE.

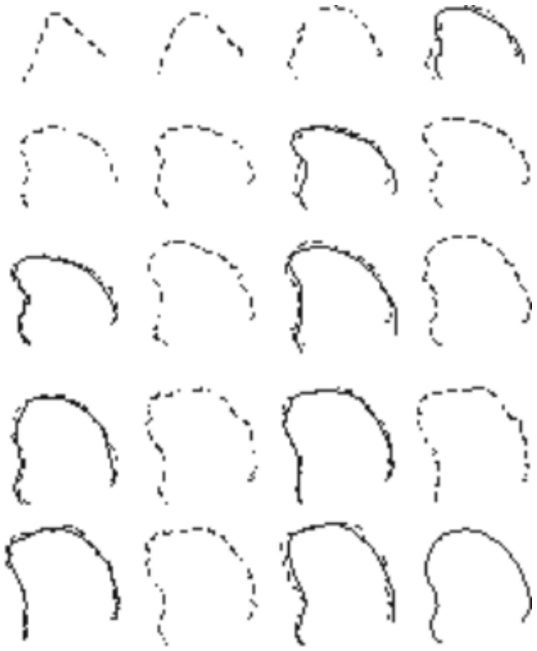

Figure 21. Snake contours (dashed) and constrained contours (continuous) with increasing number of iterations (left to right, top to bottom). Reprinted with permission from [62].

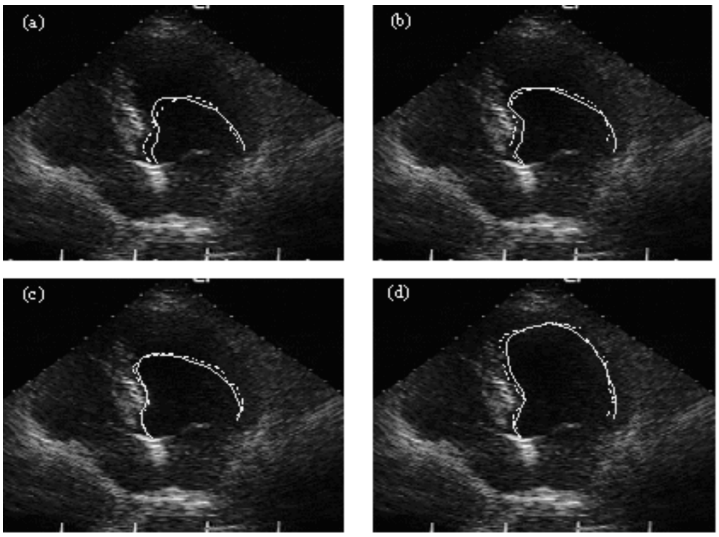

Figure 22. Progress ((a)–(d)) of a snake overlain on an ultrasound image of the left ventricle (dashed), and the result of DCT–Truncation–Projection–IDCT (continuous). Reprinted with permission from [62]. Copyright ©2000, IEEE.

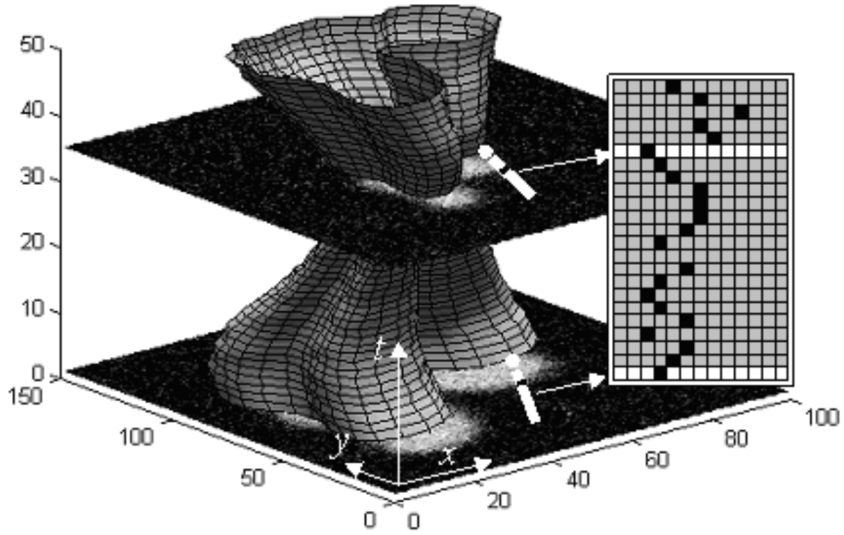

(a)

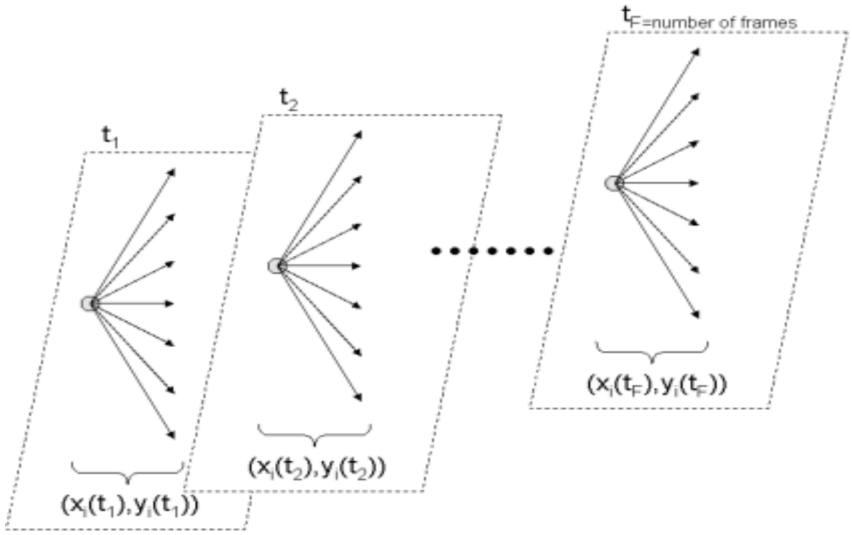

(b)

Figure 23. Proposing a new ST shape. (a) An illustration of an ST shape overlain on an image sequence. The search profiles of one landmark in two frames are shown in white. Examples of proposed landmark positions are shown as black squares. (b) The different choices of the new positions of landmark i in all frames. Reprinted with permission from [63]. Copyright ©2004, Elsevier.

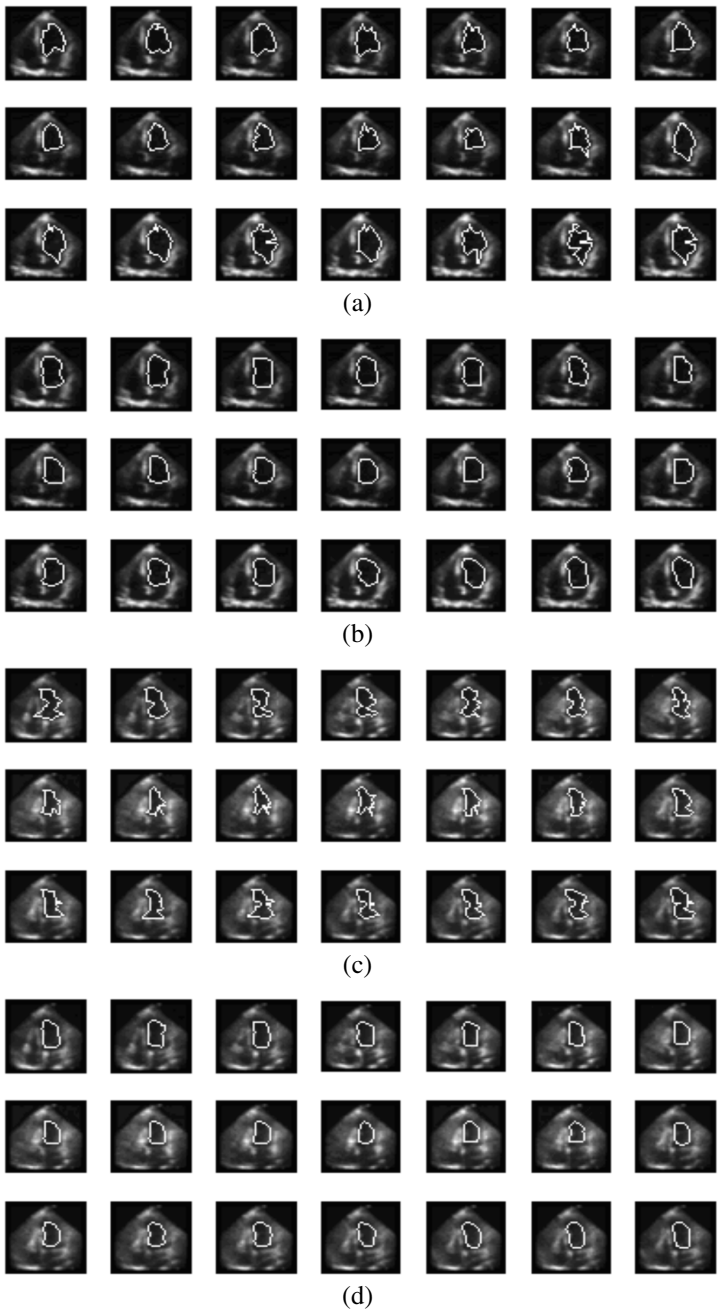

Figure 24. Left-ventricular segmentation result from two echocardiographic image sequences. Ultrasound frames are shown with the ST shape overlain (a,c) before and (b,d) after projection onto the ASTSD (frames progress from left to right, top to bottom). Reprinted with permission from [63]. Copyright ©2004, Elsevier.

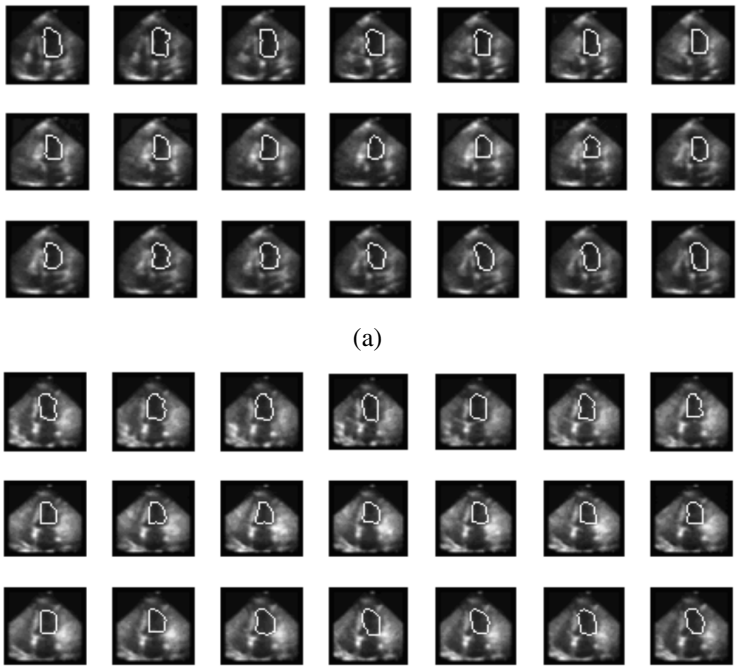

Figure 25. Additional left-ventricular segmentation results from an echocardiographic image sequence (frames progress from left to right, top to bottom). Reprinted with permission from [63].

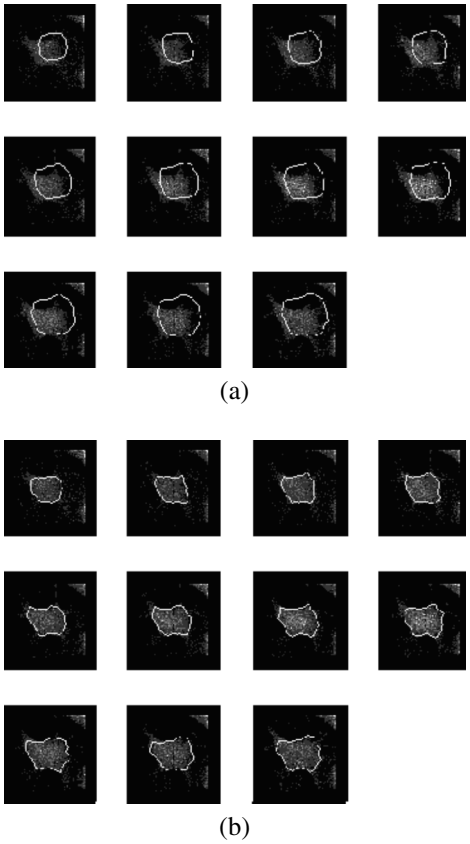

Figure 26. Segmenting a 3D astrocyte cell (spatial z-axis replaces time): (a) initial shape model and (b) segmentation result overlain in white on a fluorescence 3D image. Reprinted with permission from [63]. Copyright ©2004, Elsevier.